

K-shell photoionization of Li, Be⁺ and B²⁺

Jun Li,* Jian Dang Liu,* Song Bin Zhang,^{†,‡,§,¶} and Bang Jiao Ye*,^{||}

*State Key Laboratory of Particle Detection and Electronics,
Department of Modern Physics,

University of Science and Technology of China, 230026 Hefei, China

[†]School of Physics and Information Technology,
Shaanxi Normal University, 710119 Xian, China

[‡]Max Planck Institute for the Structure and Dynamics of Matter (MPSD),
22761 Hamburg, Germany

[§]Center for Free-Electron Laser Science (CFEL), 22761 Hamburg, Germany

[¶]song-bin.zhang@snnu.edu.cn

^{||}bjye@ustc.edu.cn

Received 18 December 2015

Revised 2 February 2016

Accepted 2 March 2016

Published 1 June 2016

K-shell photoionization (PI) of Li, Be⁺ and B²⁺ from ground state $1s^2 2s^2 S^e$ have been studied by using the R -matrix method with pseudostates. The K-shell PI process is featured with the contributions from the core-excited metastable states or dominated by the Auger states $2P^o$. The resonant parameters of the Auger states $2P^o$ and the PI cross-sections have been calculated and compared with the available experimental and theoretical works. Our results agree very well with that of the published works. It is worth noting that compared with previous theoretical calculations, our results of B²⁺ show better agreements with the latest high-resolution advanced light source measurements [A. Müller *et al.*, *J. Phys. B* **43** (2010) 135602].

Keywords: K-shell photoionization; R -matrix; Auger states.

1. Introduction

Thanks to the satellites such as *Chandra* and *XMM-Newton*, an abundance of X-ray spectra on many astronomical objects are currently available.¹ However, lots of high-quality atomic data are seriously needed to interpret these spectra, particularly in the K-shell energy range. It is significant to provide accurate values for K-shell photoionization (PI) cross-sections and Auger resonant parameters resulting from the photoabsorption of X-rays near the K-edge of Li and Li-like Be⁺ and B²⁺.

Many theoretical works/methods have studied the K-shell PI and Auger states of Li and Li-like ions, such as B-spline method,^{2,3} saddle-point method (SPM),^{4–11}

LS coupling *R*-matrix method.^{12–14} However, those works only partly agree well with the published experimental data. There are many experiments on the PI processes of Li,^{15–24} Be⁺,^{15,16,25–28} and B²⁺.^{10,12,15,16,26,29–31} It is worth mentioning that based on the advanced light source (ALS) synchrotron radiation facility, recently Müller *et al.*¹² have achieved the high resolution K-shell PI spectra of B²⁺, and the resonant parameters of the ²P^o Auger states in a high accuracy. Using the *R*-matrix with pseudo-states (RMPS), the present theoretical work studies the K-shell PI cross-sections and resonant parameters of ²P^o Auger states of Li, Be⁺ and B²⁺. Our results show very good agreement with the available works, and show better agreements with the latest high-resolution ALS measurements¹² compared with other theoretical calculations. The theoretical method is briefly presented in Sec. 2, followed with the numerical results in Sec. 3, the conclusion is given in Sec. 4. Atomic units will be used if otherwise not stated explicitly.

2. Theory

The *R*-matrix method is employed in this work. The *R*-matrix theory for photon-atom and electron-atom interactions has been discussed in detail by Burke,³² here we will give only a brief description of it. The basic idea of *R*-matrix theory is to divide the coordinate space into three regions, an inner region, an outer region and an asymptotic region. In the internal region, the scattering electron (or photo electron) is indistinguishable from the electrons of the target, the short-range, exchange and correlation interactions between the scattering electron (or photo electron) and target electrons are completely taken into account in this region. The wave function of the (*N* + 1)-electron system in the internal region is expanded in a configuration interaction basis:³³

$$\begin{aligned} \psi_k(x_1, \dots, x_{N+1}) = & A \sum_{ij} c_{ijk} \bar{\Phi}_i(x_1, \dots, x_N; \hat{\mathbf{r}}_{N+1} \sigma_{N+1}) \times \frac{1}{r_{N+1}} u_{ij}(r_{N+1}) \\ & + \sum_j d_{jk} \chi_j(x_1, \dots, x_{N+1}), \end{aligned} \quad (1)$$

where *A* is the antisymmetrization operator accounting for the exchange between the scattering electron (or photo electron) and the target electrons. The functions $\bar{\Phi}_i$ are formed by coupling the target states with the angle and spin functions of the scattering electron (or photo electron). u_{ij} are radial functions of the scattering electron (or photo electron), and χ_j are square-integrable correlation functions to ensure completeness of the total wave functions. The coefficients c_{ijk} and d_{jk} are obtained by diagonalizing the (*N* + 1)-electron Hamiltonian in the basis ψ_k .

In the external region, the electron exchange and correlation effects between the incident (or outgoing) and target electrons are negligible, only the long-range local multipole potential of the target atom (or ion) plays an important role on the scattered electron (or photo electron), whose motions can be described by a set of coupled second-order differential equations with the long-range local multipole

potential of the target atom (or ion). The coupled equations and the wave functions can be solved considering the boundary conditions in the asymptotic region. Finally, the R -matrix is determined by matching the solutions at the boundary between the inner and outer regions, and the wave function of $(N + 1)$ -electron system in the whole space is solved.³³

To calculate the PI cross-section, we also need to determine the line strength, which in length gauge is obtained from the reduced dipole matrix³³ by

$$S_L(E_f; i) = \sum_{Ll_f} |(Ll_f E_f || D_L || i)|^2 \quad (2)$$

for a transition from an initial bound state i of energy E_i to a final free state f of energy $E_f = E_i + \omega$, where ω is the photon energy in Ryd and D_L is the dipole length operator. The PI cross-section is given by

$$\sigma = \frac{4}{3} \pi^2 a_0^2 \alpha^2 \frac{\omega}{g_i} S_L, \quad (3)$$

where a_0 is the Bohr radius, α is the fine-structure constant, g_i is the statistical weight of the initial bound state.

The resonant parameters have been determined by fitting the eigenphase sum to the Breit–Wigner resonance form:^{34,35}

$$\delta = -\arctan\left(\frac{\Gamma/2}{E - E_r}\right), \quad (4)$$

where δ is the phase shift, Γ is the resonant width and E_r is the resonant position. The above expression also tells Γ can be determined from

$$\Gamma = 2/\delta'(E_r). \quad (5)$$

Generally, the point of maximum gradient $\delta'(E)$ serves as definition for the position of the resonance, and the width can be determined from Eq. (5). In the calculation, we have used an energy grid of 10^{-4} Ryd throughout the energy region considered, but in the vicinity of some resonances we have even refined it to 10^{-8} Ryd in order to accurately obtain the resonant parameters.

3. Numerical Results

The Belfast atomic R -matrix packages³³ are employed to do the scattering calculations, the target wave functions are optimized and prepared with AUTOSTRUCTURE^{36,37} in LS coupling level. During the orbital optimization with AUTOSTRUCTURE, 6 spectroscopic orbitals ($1s, 2s, 3s, 2p, 3p, 3d$) are determined by using the Thomas–Fermi–Dirac–Amaldi model potential,³⁸ and 12 pseudo-orbitals ($4\bar{s}-7\bar{s}, 4\bar{p}-7\bar{p}, 4\bar{d}-7\bar{d}$) are generated from a set of non-orthogonal Laguerre orbitals³⁹

$$P_{nl}(r) = N_{nl}(\lambda_{nl} z r)^{l+1} e^{-\lambda_{nl} z r/2} L_{n+l}^{2l+1}(\lambda_{nl} z r), \quad (6)$$

Table 1. Energy level (Ryd) of target ion Li^+ .

No.	Configuration	AUTOSTRUCTURE	NIST ⁴⁰	Difference (%)
1	$1s^2 \ ^1S$	0.000000	0.000000	0.00
2	$1s2s \ ^3S$	4.339730	4.337949	0.04
3	$1s2s \ ^1S$	4.477728	4.477734	0.00
4	$1s2p \ ^3P$	4.496387	4.504039	-0.17
5	$1s2p \ ^1P$	4.571950	4.572816	-0.02
6	$1s3s \ ^3S$	5.095184	5.055294	0.79
7	$1s3s \ ^1S$	5.112519	5.091958	0.40
8	$1s3p \ ^3P$	5.112897	5.098542	0.28
9	$1s3d \ ^3D$	5.118073	5.114423	0.07
10	$1s3d \ ^1D$	5.142082	5.114701	0.54
11	$1s3p \ ^1P$	5.147587	5.119068	0.56

Table 2. Energy level (Ryd) of target ion Be^{2+} .

No.	Configuration	AUTOSTRUCTURE	NIST ⁴⁰	Difference (%)
1	$1s^2 \ ^1S$	0.000000	0.000000	0.00
2	$1s2s \ ^3S$	8.719189	8.716288	0.03
3	$1s2s \ ^1S$	8.941147	8.941152	0.00
4	$1s2p \ ^3P$	8.953138	8.960990	-0.09
5	$1s2p \ ^1P$	9.089415	9.089470	0.00
6	$1s3s \ ^3S$	10.278181	10.216980	0.60
7	$1s3s \ ^1S$	10.307824	10.276404	0.31
8	$1s3p \ ^3P$	10.308689	10.281826	0.26
9	$1s3d \ ^3D$	10.318162	10.309920	0.08
10	$1s3d \ ^1D$	10.367711	10.310640	0.55
11	$1s3p \ ^1P$	10.381133	10.319097	0.60

where $z = Z - N + 1$, Z is the nuclear charge and N is the number of target electrons. L_{n+l}^{2l+1} represents the Laguerre polynomial and N_{nl} is a normalization constant. These Laguerre orbitals were then orthogonalized to each other and to the spectroscopic orbitals. The scaling parameters λ_{nl} can adjust the energy levels and the radial extent of the pseudo-orbitals.³⁹ For systems Li^+ , Be^{2+} and B^{3+} , the scaling parameter λ_{4s} is changed to optimize $1s2s \ ^1S$ state, so that its energy level is close to that presented in NIST.⁴⁰ We list the first 11 physical target energy levels in Tables 1–3, and compare with the NIST atomic spectra database,⁴⁰ we can see the differences of levels are all less than 1% (the difference is defined as $\frac{E_{\text{AUTO}} - E_{\text{NIST}}}{E_{\text{NIST}}} \times 100\%$). In the subsequent R -matrix calculations, the first 11 spectroscopic states and additional six pseudo states are retained.

K-shell PI happens once the photon energy is above the K-shell ionization threshold of the system. The K-shell thresholds for Li , Be^+ and B^{2+} are 50.975 eV, 96.106 eV and 154.812 eV, respectively.⁴¹ Figure 1 shows the calculated K-shell PI cross-sections for Li , Be^+ and B^{2+} . As the figure clearly shows, the K-shell PI cross-

Table 3. Energy level (Ryd) of target ion B³⁺.

No.	Configuration	AUTOSTRUCTURE	NIST ⁴⁰	Difference (%)
1	1s ² ¹ S	0.000000	0.000000	0.00
2	1s2s ³ S	14.598524	14.594234	0.03
3	1s2s ¹ S	14.905689	14.905689	0.00
4	1s2p ³ P	14.908425	14.916617	-0.05
5	1s2p ¹ P	15.109005	15.108550	0.00
6	1s3s ³ S	17.239073	17.156789	0.48
7	1s3s ¹ S	17.281396	17.239095	0.25
8	1s3p ³ P	17.282903	17.243205	0.23
9	1s3d ³ D	17.296813	17.283838	0.08
10	1s3d ¹ D	17.401959	17.285169	0.68
11	1s3p ¹ P	17.421256	17.297835	0.71

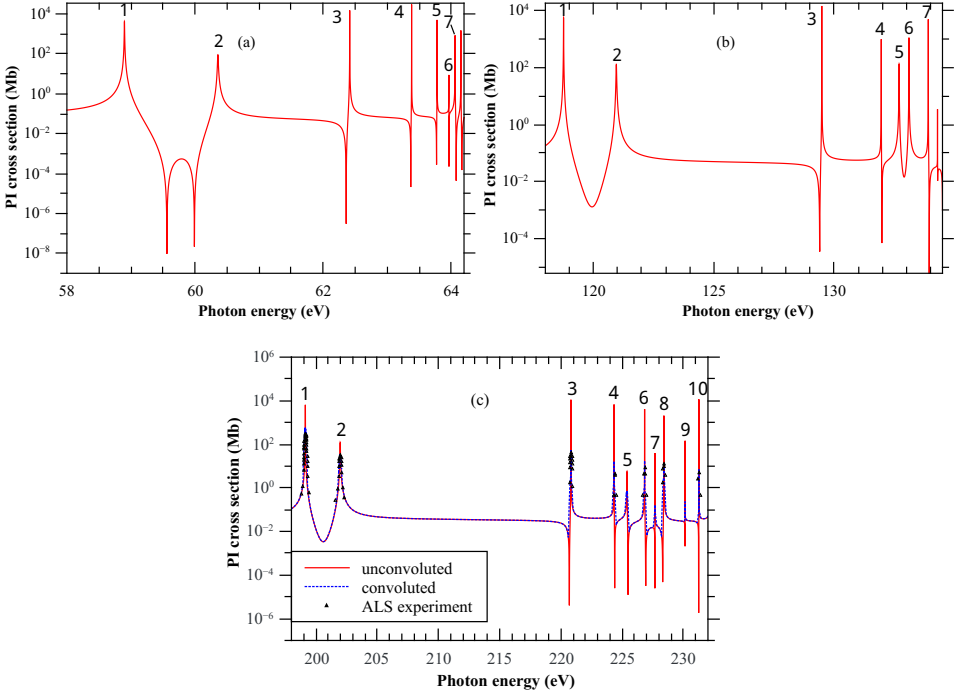


Fig. 1. (Color online) Calculated K-shell photoionization (PI) cross-sections of (a) Li, (b) Be⁺ and (c) B²⁺. The convoluted results are performed with a Gaussian distribution function of 135 meV full width at half maximum of the ALS experimental data.¹²

sections are dominated by many peaks, and the corresponding first three peaks for the Li and Li-like systems show similar structures. The shape of the resonance is determined by the Fano factors.⁴² Those peaks are contributed by the Auger states of Li and Li-like systems. At some specific incident energy, the photon can also

Table 4. Resonant positions (eV) of Auger states $^2P^o$ of B^{2+} .

No.	Configuration ($^2P^o$)	Experiment ¹²	R -matrix (present)	R -matrix ¹²	B-spline ²	Saddle-point ⁴
1	$1s(2s2p\ ^3P)$	199.149 ± 0.030	$199.136(-0.0065\%)$	$199.092(-0.0286\%)$	$199.145(-0.0020\%)$	$199.181(0.0161\%)$
2	$1s(2s2p\ ^1P)$	201.987 ± 0.030	$201.979(-0.0040\%)$	$201.991(0.0020\%)$	$202.024(0.0183\%)$	$202.041(0.0267\%)$
3	$(1s2s\ ^3S)3p$	220.823 ± 0.030	$220.814(-0.0041\%)$	$220.721(-0.0462\%)$	$220.826(0.0014\%)$	$220.851(0.0127\%)$
4	$(1s2s\ ^1S)3p$	224.411 ± 0.030	$224.334(-0.0343\%)$	$224.301(-0.0490\%)$	$224.416(0.0022\%)$	$224.476(0.0290\%)$
5	$(1s2p\ ^3P)3s$	—	225.392	225.407	225.482	225.554
6	$(1s2p\ ^1P)3s$	226.834 ± 0.030	$226.828(-0.0026\%)$	$226.791(-0.0190\%)$	$226.849(0.0066\%)$	—
7	$(1s2p\ ^3P)3d$	—	227.677	227.731	227.760	—
8	$(1s2p\ ^1P)3d$	228.394 ± 0.030	$228.404(0.0044\%)$	$228.371(-0.0101\%)$	—	—
9	$1s(3s3p\ ^3P)$	—	230.135	—	—	—
10	$1s(3s3p\ ^1P)$	231.233 ± 0.030	$231.260(0.0117\%)$	$231.201(-0.0138\%)$	—	—

Table 5. Resonant positions (eV) of Auger states ²P^o of Be⁺.

No.	Configuration (² P ^o)	Experiment ²⁵	<i>R</i> -matrix (present)	B-spline ²	Saddle-point ⁵
1	1s(2s2p ³ P)	118.74(3)	118.756(0.0135%)	118.761(0.0177%)	118.778(0.0320%)
2	1s(2s2p ¹ P)	120.95(1)	120.948(-0.0017%)	120.996(0.0380%)	120.998(0.0397%)
3	(1s2s ³ S)3p	129.509(7)	129.484(-0.0193%)	129.491(-0.0139%)	129.495(0.0108%)
4	(1s2s ¹ S)3p	132.00(3)	131.956(-0.0333%)	132.014(0.0106%)	132.050(0.0379%)
5	(1s2p ³ P)3s	132.70(1)	132.697(-0.0023%)	132.746(0.0347%)	132.783(0.0625%)
6	(1s2s ³ S)4p	133.07(3)	133.106(0.0271%)	133.122(0.0391%)	133.130(0.0451%)
7	(1s2p ¹ P)3s	133.99(9)	133.910(-0.0597%)	133.916(-0.0552%)	133.930(0.0448%)

Table 6. Resonant positions (eV) of Auger states ²P^o of Li.

No.	Configuration (² P ^o)	Experiment ²⁴	<i>R</i> -matrix (present)	B-spline ²	Saddle-point ⁶
1	1s(2s2p ³ P)	58.908(3)	58.898(-0.0170%)	58.908(0.0000%)	58.910(0.0034%)
2	1s(2s2p ¹ P)	60.392(3)	60.357(-0.0580%)	60.407(0.0248%)	60.398(0.0099%)
3	(1s2s ³ S)3p	62.417(3)	62.415(-0.0032%)	62.421(0.0064%)	62.417(0.0000%)
4	(1s2s ³ S)4p	63.357(3)	63.381(0.0379%)	63.356(-0.0016%)	63.351(-0.0095%)
5	(1s2s ³ S)5p	63.755(3)	63.778(0.0361%)	63.753(-0.0031%)	63.750(-0.0078%)
6	(1s2s ³ S)6p	63.956(3)	63.963(0.0109%)	63.953(-0.0047%)	63.950(-0.0094%)
7	(1s2s ³ S)7p	64.051(3)	64.060(0.0141%)	64.062(0.0172%)	64.050(-0.0016%)

excite the K-shell electron and form a highly excited metastable state or Auger state, which Auger decays and manifests as a peak in the PI cross-sections. Note that after doing the convolution with a Gaussian distribution function of 135 meV full width at half maximum, the calculated cross-sections of B²⁺ also agree very well with the latest high resolution experimental data¹² (see Fig. 1).

Auger states are very important participants in the K-shell PI process, it is significant to study the resonant parameters for those states. Tables 4–6 present the present calculated resonant energies of B²⁺, Be⁺ and Li, respectively, together with the experimental data^{12,24,25} and other theoretical calculations.^{2,4–6,12} As shown in the tables, the present results agree very well with the experimental data, most of the resonant positions calculated are within 1% difference from the experimental data (the difference is defined as $\frac{E_{\text{cal.}} - E_{\text{exp}}}{E_{\text{exp}}} \times 100\%$). Especially for B²⁺, the present *R*-matrix calculations show best agreements with the latest high resolution ALS measurements¹² than other theoretical results, including the previous *R*-matrix calculations.¹² B-spline² and saddle-point⁶ methods calculate the resonant positions more accurately for Li than the present *R*-matrix method. It comes from the fact that for Li, the Auger states are mostly formed by exciting the inner shell electron into the Rydberg orbitals, which cannot be easily optimized in *R*-matrix calculations.

Table 7. Resonant widths (eV) of Auger states $2P^o$ of B^{2+} .

No.	Configuration ($2P^o$)	R -matrix				
		Experiment ¹²	(present)	R -matrix ¹²	B-spline ²	Saddle-point ⁴
1	$1s(2s2p\ ^3P)$	4.8 ± 0.6	4.8587	4.40	4.29	4.05
2	$1s(2s2p\ ^1P)$	29.7 ± 2.5	30.8490	30.53	30.52	30.60
3	$(1s2s\ ^3S)3p$	—	0.4510	0.50	0.46	0.381
4	$(1s2s\ ^1S)3p$	—	0.2416	0.28	0.26	0.21
5	$(1s2p\ ^3P)3s$	—	11.8598	11.39	11.39	11.32
6	$(1s2p\ ^1P)3s$	—	0.4178	0.46	0.470	—
7	$(1s2p\ ^3P)3d$	—	0.4119	0.59	0.463	—
8	$(1s2p\ ^1P)3d$	—	0.6831	0.66	—	—
9	$1s(3s3p\ ^3P)$	—	0.1576	—	—	—
10	$1s(3s3p\ ^1P)$	—	0.0601	0.07	—	—

Table 8. Resonant widths (eV) of Auger states $2P^o$ of Be^+ .

No.	Configuration ($2P^o$)	R -matrix		
		(present)	B-spline ²	Saddle-point ⁵
1	$1s(2s2p\ ^3P)$	4.6438	4.26	4.38
2	$1s(2s2p\ ^1P)$	21.9104	20.87	20.4
3	$(1s2s\ ^3S)3p$	0.3187	0.32	0.32
4	$(1s2s\ ^1S)3p$	0.3849	0.40	0.45
5	$(1s2p\ ^3P)3s$	6.1357	5.01	5.28
6	$(1s2s\ ^3S)4p$	1.9838	3.03	3.24
7	$(1s2p\ ^1P)3s$	0.2434	0.17	0.23

The resonant widths for B^{2+} , Be^+ and Li are presented in Tables 7–9, respectively. Only limited experimental data existed for the first two Auger states of B^{2+} , as shown in Table 7, our calculations agree very well with those experimental data, and also other theoretical results. Tables 8 and 9 show that all the three theoretical methods (R -matrix, B-spline and saddle-point) produce the close results. Lots of efforts are taken during the orbital optimization, and the present R -matrix calculations are generally better than the previous one. For the resonance $1s2s(^3S)4p$ of Be^+ , the width of other calculations could be more reliable, since it is quite difficult to get balance during the optimization of $4p$ orbital in R -matrix calculations. However, more high resolution experiments are required to finally determine those Auger widths. The first three Auger states of Li , Be^+ and B^{2+} possess the same type or configuration. Tables 7–9 also show that the resonant widths for the same type Auger states increase with the increase of the nuclear charge of Li , Be^+ and B^{2+} , which is consistent with the statements in Ref. 43.

Table 9. Resonant widths (eV) of Auger states ²P^o of Li.

No.	Configuration (² P ^o)	R-matrix (present)	B-spline ²	Saddle-point ⁶
1	1s(2s2p ³ P)	3.9916	3.78	3.33
2	1s(2s2p ¹ P)	10.5197	9.97	9.56
3	(1s2s ³ S)3p	0.2143	0.20	0.203
4	(1s2s ³ S)4p	0.0374	0.04	0.0445
5	(1s2s ³ S)5p	0.0638	0.05	0.0445
6	(1s2s ³ S)6p	0.3081	0.15	0.140
7	(1s2s ³ S)7p	0.3826	0.50	0.391

4. Conclusions

K-shell photoionization of Li, Be⁺ and B²⁺ from ground state 1s²2s ²S^e have been studied by using the *R*-matrix method with pseudostates. K-shell excited Auger states ²P^o dominate the PI cross-sections. Both the PI cross-sections and the resonant parameters (positions and widths) are reported and compared with the available experimental and theoretical data. Our results show good agreement with the published works. Especially for B²⁺, our present calculations show best agreement than other calculations with the latest high resolution ALS measurements.

Acknowledgments

The authors acknowledge W. S. Zhang for his valuable discussions. S. B. Zhang was partly supported by the Max-Planck Scholarship and the starting grants of Shaanxi Normal University (Grant Nos. 1112010214 and 1110010733). B. J. Ye was supported by the National Natural Science Foundation of China (Grant Nos. 11175171 and 11475165).

References

1. B. M. McLaughlin, C. P. Ballance, K. P. Bowen, D. J. Gardenghi and W. C. Stolte, *Astrophys. J. Lett.* **771** (2013) L8.
2. G. Verbockhaven and J. E. Hansen, *J. Phys. B* **34** (2001) 2337.
3. O. Zatsarinny and C. F. Fischer, *J. Phys. B* **33** (2000) 313.
4. B. F. Davis and K. T. Chung, *Phys. Rev. A* **31** (1985) 3017.
5. Z. Liu, L. Wu and B. Li, *J. Phys. B* **32** (1999) 3899.
6. K. T. Chung, *Phys. Rev. A* **56** (1997) R3330.
7. M.-K. Chen and K. T. Chung, *Phys. Rev. A* **49** (1994) 1675.
8. K. T. Chung, *Phys. Rev. A* **57** (1998) 3518.
9. L. Wu and J. Xi, *J. Phys. B* **24** (1991) 3351.
10. K. T. Chung and R. Bruch, *Phys. Rev. A* **28** (1983) 1418.
11. G. Bingcong and D. Wensheng, *Phys. Rev. A* **62** (2000) 032705.
12. A. Müller, S. Schippers, R. A. Phaneuf, S. W. J. Scully, A. Aguilar, C. Cisneros, M. F. Gharaibeh, A. S. Schlachter and B. M. McLaughlin, *J. Phys. B* **43** (2010) 135602.
13. S. N. Nahar, A. K. Pradhan and H. L. Zhang, *Astrophys. J. Suppl. Ser.* **131** (2000) 375.

14. S. N. Nahar, *J. Quant. Spectrosc. Radiat. Transfer* **117** (2013) 15.
15. R. Bruch, G. Paul, J. Andrä and B. Fricke, *Phys. Lett. A* **53** (1975) 293.
16. M. Rodbro, R. Bruch and P. Bisgaard, *J. Phys. B* **12** (1979) 2413.
17. D. J. Pegg, H. H. Haselton, R. S. Thoe, P. M. Griffin, M. D. Brown and I. A. Sellin, *Phys. Rev. A* **12** (1975) 1330.
18. P. Ziem, N. Stolterfoht and R. Bruch, *J. Phys. B* **8** (1975) L480.
19. D. Rassi, V. Pejcev and K. J. Ross, *J. Phys. B* **10** (1977) 3535.
20. L. M. Kiernan, M.-K. Lee, B. F. Sonntag, P. Zimmermann, J. T. Costello, E. T. Kennedy, A. Gray and L. V. Ky, *J. Phys. B* **29** (1996) L181.
21. T. J. McIlrath and T. B. Lucatorto, *Phys. Rev. Lett.* **38** (1977) 1390.
22. D. L. Ederer, T. Lucatorto and R. P. Madden, *Phys. Rev. Lett.* **25** (1970) 1537.
23. S. Mannervik and H. Cederquist, *Phys. Scripta* **31** (1985) 79.
24. A. M. Cantù, W. H. Parkinson, G. Tondello and G. P. Tozzi, *J. Opt. Soc. Am.* **67** (1977) 1030.
25. E. Jannitti, M. Mazzoni, P. Nicolosi, G. Tondello and W. Yongchang, *J. Opt. Soc. Am. B* **2** (1985) 1078.
26. E. T. Kennedy and P. K. Carroll, *J. Phys. B* **11** (1978) 965.
27. A. E. Kramida, *Phys. Scripta* **57** (1998) 66.
28. M. Agentoft, T. Andersen, C. F. Fischer and L. Smentek-Mielczarek, *Phys. Scripta* **28** (1983) 45.
29. Y. Baudinet-Robinet, P. Dumonta, H. Garnir, E. Träbert and P. Heckmann, *Z. Phys. D* **7** (1987) 47.
30. A. E. Kramida, A. N. Ryabtsev, J. O. Ekberg, I. Kink, S. Mannervik and I. Martinson, *Phys. Scripta* **78** (2008) 025301.
31. E. Jannitti, P. Nicolosi and G. Tondello, *Physica B+C* **124** (1984) 139.
32. P. Burke, *R-Matrix Theory of Atomic Collisions: Application to Atomic, Molecular and Optical Processes*, Springer Series on Atomic, Optical, and Plasma Physics (Springer, 2011).
33. K. A. Berrington, W. B. Eissner and P. H. Norrington, *Comput. Phys. Commun.* **92** (1995) 290.
34. H. Friedrich and H. Friedrich, *Theoretical Atomic Physics* (Springer, 2006).
35. S. B. Zhang, J. G. Wang and R. K. Janev, *Phys. Rev. A* **81** (2010) 032707.
36. N. Badnell, *Comput. Phys. Commun.* **182** (2011) 1528.
37. W. Eissner, M. Jones and H. Nussbaumer, *Comput. Phys. Commun.* **8** (1974) 270.
38. N. R. Badnell, *J. Phys. B* **30** (1997) 1.
39. P. R. Berman, C. C. Lin and E. Arimondo, *Advances in Atomic, Molecular, and Optical Physics* (Academic Press, 2006).
40. A. Kramida et al., National Institute of Standards and Technology, Gaithersburg, MD, 2012.
41. S. B. Zhang and D. L. Yeager, *J. Mol. Struct.* **1023** (2012) 96.
42. U. Fano, *Phys. Rev.* **124** (1961) 1866.
43. A. K. Bhatia, *Phys. Rev. A* **18** (1978) 2523.